VOL. 11, NO. 19, OCTOBER 2016 ISSN 1819-6608
ARPN Journal of Engineering and Applied Sciences

www.arpnjournals.com

NUMERICAL AND EXPERIMENTAL ANALYSIS OF TRANSIENT TEMPERATURE AND RESIDUAL THERMAL STRESSES IN FRICTION STIR WELDING OF ALUMINUM ALLOY 7020-T53

Muhsin J. J.[1], Moneer H. Tolephih[2] and Muhammed A. M.[1] and Ghanim Sh. Sadiq[1]
[1]Department of Mechanical Engineering, Al-Nahrain University/College of Engineering, Iraq
[2]Department of Mechanical Engineering, Karbala University/College of Engineering, Iraq
E-Mail: ghanim_sadiq@yahoo.com

ABSTRACT

Plates of aluminum alloys 7020-T53 were joined in a butt joint by friction stir welding. The residual stresses were measured using the hole-drilling strain-gauge method on the mid position of welding line at three places (advance side, nugget and retreate side). In this investigation, three-dimensional numerical simulation of friction stir welding was concerned to study the influence of tool moving speed in relation with heat distribution as well as residual stress. Simulation was composed of two stages. Firstly, transient temperature distribution on the workpiece while undergoing the welding process was studied. In the second stage, attained thermal behavior of the piece from previous stage is considered as inlet heat of an elasto-plastic, thermomechanical model for the prediction of residual stress. In experimental results, the temperatures are higher on the advancing side than the retreating side along welding, and it was found that the residual stresses on the advance side at about 116.61MPa, while the value reached 90.84MPa for the weld at nugget in retreate side residual stress was107.5MPa and numerical results had the conventional ‘‘M’’ profile with tensile stress peaks in the heat-affected zone.

Keywords: friction stir welding, residual stress, transient temperature, temperature distribution and simulation.

1. INTRODUCTION

Friction stir welding (FSW) is a relatively contemporary solid-state process introduced back in 1991 by TWI [1]. Based on its advantages, this welding procedure has become more popular recently. Some of these advantages include, however, not limited to the following: low shrinkage and distortion, desired mechanical properties, producing less fumes, and ability in welding of alloys otherwise difficult with other melting welding procedures, alloys such as 2xxx and 7xxx series of aluminum [2]. It could safely be stated that most if not all abovementioned advantages are due to the fact that the generated heat produced by the process remains below melting temperature of the metal. Consequently, undesired parameters resulted from typical welding processes will not materialize. Some of these parameters are solidification cracking, liquidation cracking, and porosity.

Fundamental of friction stir welding is depicted in Figure-1. In this procedure, two plates are firmly clamped on the backing plate. Spinning tool slowly lowers into the connecting plates until tool shoulder touches the upper surfaces of the plates. While spinning, the moving displaces forward on the piece and this causes heat due to the friction between them. The tool starts to move after pausing for warm-up of the plates. While forward moving, the tool forges the materials by spinning and as result, a strong connection will take place between the plates. In some cases, in order to provide more effective forge due to better string of the materials, the tool is somewhat angled from its vertical position.

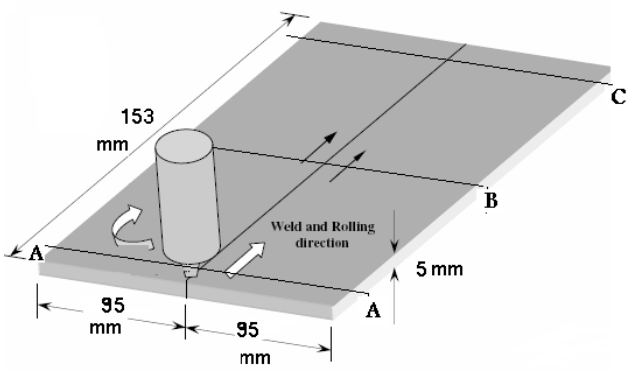

Figure-1. A schematic illustration of the friction stir welding process.

Plates in which rotation and movement direction of the tool are the same is caused advancing side and the other plate is known as retreating side [3]. Difference between relative speed of the tool and plates surfaces on both sides will cause variation in the amount of generated heat distribution. There are many variations in the process of FSW that makes it difficult to conduct a thrill investigation. Major, independent variables are: rotational speed of the tool, tool advancing speed, magnitude of downward force to hold the touch between tool and piece steady, tool geometry, and tilt angle. These variables affect heat distribution as well as residual stress and mechanical properties of the connection. Consequently, numerical simulation could be a helpful device for predicting process behavior and its optimization. In friction stir welding, heat is generated first on the basis of friction between tool and work piece and then by shape change. A portion of the

generated heat disseminated through work piece, will affect distortion, residual stress distribution as well as weld quality of the piece. Chao *et al.* [4] and Muhammed *et al.* [31] investigated the variations of heat energy and temperature produced by the FSW in both the work piece and the tool. The most striking result from their study is that only about 5% of the heat generated by the friction process flows to the tool and the rest flows to the work piece. To date, most of the researches have been done on the heat transfer of FSW. Schmidt *et al.* [5] proposed a general analytical model for heat generation based on two contact conditions at the tool/matrix interface, namely full sliding and full sticking condition. In the case of sliding, the heat was applied as a surface flux, and in the case of sticking, the heat was applied as a volume flux in a shear layer. Mandal *et al.* [6] provided a theoretical framework for developing a thermo-mechanical hot channel approach for augmenting the FSW process. Song *et al.* [7] used a three dimensional heat transfer model to predict the temperature distributions in FSW. They assume that heat generated at the tool shoulder/work piece interface is frictional heat and the plastic strain is negligible. Zhang *et al.* [8-10] used the two- and three-dimensional thermo-mechanical model to analyze the material flows, temperature history and mechanical features in the FSW process. Nandan *et al.* [11, 12] have modeled a Three-dimensional visco-plastic flow of metals and the temperature fields in friction stir welding of 6061 aluminum alloy and 304L austenitic stainless steel. They numerically simulated the temperature fields, cooling rates, and the geometry of the thermo-mechanically affected zone (TMAZ) using heat generation rates and non- Newtonian viscosity. In their study the heat generation rate was calculated from the tool geometry, rotational speed, and shear stress for yielding and the spatial variation of non-Newtonian viscosity was determined from the computed values of strain rate, temperature, and material properties. The computed temperature versus time plots and the geometry of the TMAZ region agreed well with corresponding independent experimental results. Residual stresses are defined as the stresses that remain in structures after removing the external forces and thermal gradients. It is known that the compressive residual stresses increase the fatigue life and corrosion resistance. John *et al.* [13] and Bussu and Irving [14] have investigated the effects of weld residual stress on the fatigue propagation of cracks. Their comparative analysis of the results indicated that crack growth behavior in the FSW joints was generally dominated by the weld residual stress and that microstructure and hardness changes in FSWs had a minor influence. Khandkar *et al.* [15] utilized a sequentially coupled thermomechanical finite element model to study the residual stresses in friction stir welds caused by thermal cycling during FSW process, which constitute the basis of the current research. They assume that temperature distribution is symmetric about the weld line. They concluded that longitudinal stress values are the highest tensile stress components in all the cases and have values close to their room temperature yield strengths that are much more than the experimental results. Chen and Kovacevic [16] used a three-dimensional model based on finite element analysis to study the thermal history and thermo-mechanical process in the butt-welding of aluminum alloy 6061-T6. Their model was symmetry along the weld line and incorporated the mechanical reaction of the tool and thermo-mechanical process of the welded material. They assumed that the heat is generated from friction between the material and the tool and neglected any deformation heating in the weld region. Although, experimental and numerical data have shown that the material flow in FSW is not symmetric about the weld line [17, 18]. Peel *et al.* [19] reported the results of micro-structural, mechanical property, and residual stress investigations produced under varying conditions. They concluded that the weld properties were dominated by the thermal input rather than the mechanical deformation by the tool. Also, it was found out that the weld zone in FSW is in tension in both the longitudinal (parallel to tool travel) and transverse (perpendicular to tool travel) directions.

Among the papers related to the residual stresses in aluminum friction stir welds that have been published over the past several years, Linton and Ripley [20] used the neutron diffraction technique to measure residual stresses in a FSW 7xxx alloy and determine how these residual stresses change with time. It was found that the residual stresses associated with the weld nugget decreased, while those associated with the heat-affected zone increased with time. Peel *et al.* [21] have focused on observations of the weld residual stress as function of traverse speed in aluminum AA5083 using X-rays diffraction. Synchrotron residual stress analyses indicate that the weld zone is in tension in both the longitudinal (parallel to tool traverse) and transverse (perpendicular to tool traverse) directions. *The peak of the longitudinal stresses increases as the traverse speed increases*. Fratini *et al.* [22] examined the role of longitudinal residual stress on propagation of fatigue cracks in FSW produced in 2024-T351 aluminum alloy. They concluded that the fatigue crack growth behavior was dominated by residual stress outside the weld zone. However, very few direct observations of residual stress variations (including different friction stir weld zone and along the thickness plate at different welding parameters) using the hole-drilling strain-gauge method have been reported in the literature.

Objective of this study was to predict numerical thermal distribution as well as distribution of residual stress in AA 7020-T53. Plates that were welded by friction stir welding method in which welding tool rotation 1400rpm and transverse speed 40mm/min was studied. For validation of numerical predictions using ANSYS V12.0 software [23], numerical findings were compared with experimental findings using the hole-drilling strain gauge method, Meanwhile, the present study also includes temperature distribution of friction stir welded joints measured using thermocouples placed at several position of workpiece.

2. EXPERIMENTAL

The material used in this study was a consist of two 190 × 153 × 5 mm AA7020-T53 rolled plate, the butt joints were made using a special FSW machine and the welding direction was parallel to the rolling direction. The tool steel X12M consisted of an 18 mm diameter shoulder with cylinder threaded pin (M6) and 4.7 mm pin length, tool rotary speed of 1400 rpm were used in conjunction with a traverse speed of 40 mm/min.

Experiments are conduct under different welding rotational speed in order to use the measured vertical loads and temperature results for verification of the accuracy of the modeled ones, four cases are considered with differing tool rotational speeds (710rpm, 900rpm, 1120rpm and 1400rpm) is used for measuring the vertical force during the FSW process for penetration time 60sec after that tool is moving with constant axially travel speed Muhammed A.M. *et al* [31].

2.1 Temperature measurement

Temperature evolutions near the welding line were measured by the type-K thermocouples and embedded in the regions adjacent to the rotating pin underneath shoulder surface. In detail, the principle and method of temperature measurement have been carried out by the procedure as shown in Figure-2 and Figure-3. However, it is very difficult to measure the temperature in the directly stirred zone due to the intense plastic deformation produced by the rotation and translation of the tool. The depth of blind hole drilled in the cross-section of the workpiece is 7 mm from welding centre line and distance from the top surface is 1 mm Muhammed A.M. *et al* [31].

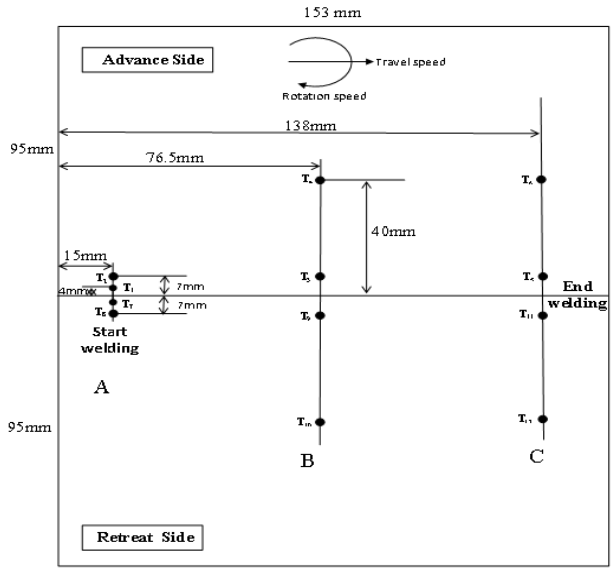

Figure-2. Thermocouple positions on the workpiece [31].

Figure-3. Temperature recorder and hole thermocouple position on workpiece [31].

The distribution of the blind holes to measure the temperature field along the welding line of plate is achieved via the following three steps. Firstly, four thermocouples in welding tool penetration, secondly, four thermocouples in mid position, third when welding tool pullout. All thermocouples were placed at advance side retreate side from the weld line in order to determine the variation with the distance to the welding line.

2.2 Residual stress measurements

The residual stresses present around the FSW were measured using the hole-drilling strain-gauge method ASTM standard E837-01 [25] , which involves drilling a hole in the center of the strain-gauge rosette, which was attached on the surface of the work piece (ground the surface using 240, 320 and 600 emery papers). In order to analyze the residual stress distribution at mid position of the plate at section B-B, the installation of the rosettes has been designed as shown in figure (4). The drill was positioned at the centre of the rosettes. Holes were drilled in depth 2 mm with a diameter of 3 mm. Meanwhile, the relieved strain caused by the drilling operation was detected by the electric resistance rosette strain gage (EA-09-125RE-120) and Strain relaxation reading was acquired by the use of 8 channels strain measuring computerized, quarter bridge circuit with (Win Daq) data acquisition devise (DI-148U sensitivity (2.5025mv/micro-strain). The three measured strain rates, ε_1, ε_2 and ε_3, were then substituted into equ. (1). Therefore, the residual principal stresses (σ_1 and σ_2); transversal and longitudinal residual stress (σ_x and σ_y) within the work piece can be calculated:

$$\sigma_{1,2} = \frac{\epsilon_1 + \epsilon_3}{4\,\bar{A}} \pm \frac{\sqrt{2}}{4\,\bar{B}} \sqrt{(\epsilon_1 - \epsilon_2)^2 + (\epsilon_1 - \epsilon_3)^2} \quad (1)$$

$$\bar{A} = -\frac{1+\upsilon}{2E\,r^2} \quad (2)$$

$$\bar{B} = -\frac{1+\upsilon}{2E\,r^2}\left(\frac{4}{1+\upsilon} - \frac{3}{r^2}\right) \quad (3)$$

$$r = \frac{D}{D_o}$$

Where $\boldsymbol{\varepsilon_1}$, $\boldsymbol{\varepsilon_2}$, $\boldsymbol{\varepsilon_3}$ are strain gages reading, D_o is the hole diameter (3mm), D is the diameter of the strain gage (10.26 mm) The angle between (σ_1) and the axis number 1, as shown in figure (5), was calculated according to the equation (4)

$$\tan(2\beta) = \frac{\epsilon_3 - 2\,\epsilon_2 + \epsilon_1}{\epsilon_3 - \epsilon_1} \quad (4)$$

$$\sigma_x = \frac{\sigma_{max} + \sigma_{min}}{2} + \frac{\sigma_{max} - \sigma_{min}}{2}\cos(2\beta) \quad (5)$$

$$\sigma_y = \frac{\sigma_{max} + \sigma_{min}}{2} - \frac{\sigma_{max} - \sigma_{min}}{2}\cos(2\beta) \quad (6)$$

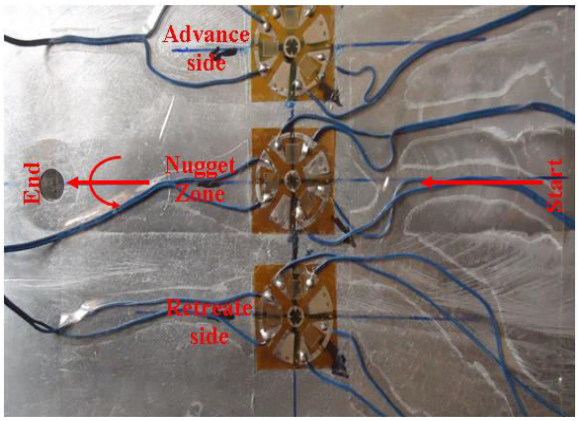

Figure-4. Strain-gauge rosette installation on the welding specimen.

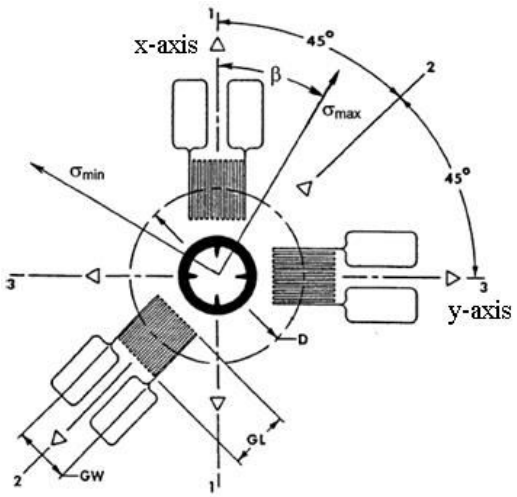

Figure-5. The direction of σ_1 with respect to x-axis and the order of gauge numbers.

The strain gage center was positioned as shown in Figure-4 in three locations the first location at 20mm from the weld center on the advancing side, the second locations in the middle of nugget zone and the third locations at 20mm from the weld centre on the retreating side these locations at mid position along welding line.

2.3 Finite element model

The model chosen for this task was the thermomechanical model developed by Nandan et al. [3] for FSW of aluminum alloy. The thermomechanical model was developed using commercial finite element analysis program ANSYS® V-12.0 [23]. In order to validate the developed model, the output of the model was correlated with experimental results. Once developed, the thermomechanical model was used to simulate the process. The model was then extrapolated to perform parametric studies in order to investigate effects of various process parameters on temperature distribution and residual stress in the workpiece.

2.4 Thermal model

The purpose of the thermal model is to calculate the transient temperature fields developed in the workpiece during friction stir welding. In the thermal analysis, the transient temperature field T which is a function of time t and the spatial coordinates (x,,), is estimated by the three dimensional nonlinear heat transfer equation (7).

$$k\left(\frac{\partial^2 T}{\partial^2 X} + \frac{\partial^2 T}{\partial^2 y} + \frac{\partial^2 T}{\partial^2 X}\right) + Q_{int} = c\rho\frac{\partial T}{\partial t} \quad (7)$$

where k is the coefficient of thermal conductivity, Q_{int} is the internal heat source rate, c is the mass-specific heat capacity, and ρ is the density of the materials, Material properties as functioned temperature as shown in Figure-6 and Figure-7.

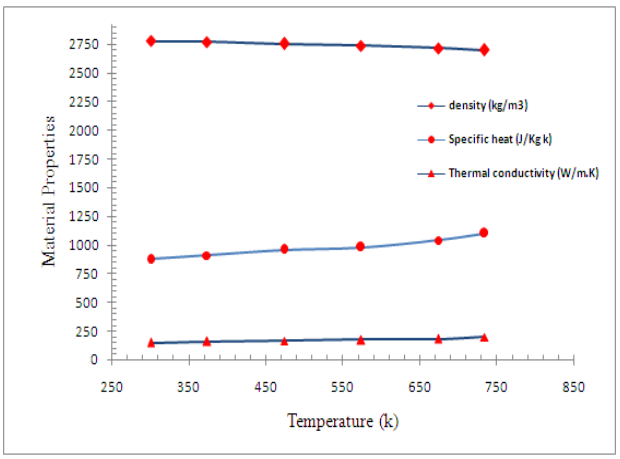

Figure-6. Variation of AA7020-T53 thermal material properties with respect to temperature [27].

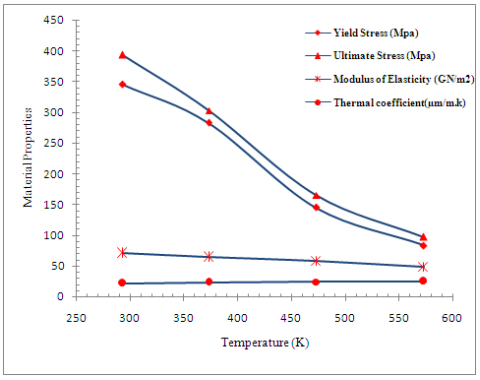

Figure-7. Variation of AA7020-T53 mechanical material properties with respect to temperature [27].

2.5 Assumptions: A number of assumptions have been made in developing the finite element thermal model, which includes:

Workpiece material is isotropic and homogeneous.

No melting occurs during the welding process.

Thermal boundary conditions are symmetrical across the weld centerline.

Heat transfer from the workpiece to the clamp is negligible.

2.6 Boundary condition

Boundary condition for FSW thermal model were specified as surface loads through ANSYS® codes. Assumptions were made for various boundary conditions based on data collected from various published research papers [26]. Convective and radiative heat losses to the ambient occurs across all free surfaces of the workpiece and conduction losses occur from the workpiece bottom surface to the backing plate. To consider convection and radiation on all workpiece surfaces except for the bottom, the heat loss q_s is calculated by equation (8).

$$q_s=\beta\ (T-T_o) +\varepsilon F\sigma(T^4-T_o^4) \quad (8)$$

where T is absolute temperature of the workpiece, T_o is the ambient temperature, β is the convection coefficient, ε is the emissivity of the plate surfaces, and $\sigma= 5.67\times10^{-8}$ W/m^2 °K^{4}is the Stefan-Boltzmann constant. In the current model, a typical value of β was taken to be 30 W/m^2K at ambient temperature of 300 K and ε was taken to be (0.5) for aluminum alloy F is radiation view factors (F=1). In order to account for the conductive heat loss through the bottom surface of weld plates, a high overall heat transfer coefficient has been assumed. This assumption is based on the previous studies [26]. The heat loss was modeled approximately by using heat flux loss by convection q_b given by equation (9).

$$q_b=\beta_b\ (T-T_o) \quad (9)$$

where β_b is a fictitious convection coefficient. Due to the complexity involved in estimating the contact condition between the welded plate and the backing plate, the value of β_b had to be estimated by assuming different values through reverse analysis approach. In this study, the optimized value of β_b was found to be (100-300) W/cm^2°C.

Heat generation during friction-stir welding arises from two main sources: deformation of the material around the tool pin and the friction at the surface of the tool shoulder. A major difficulty is determining suitable values for the friction coefficient. The conditions under the tool are both extreme and very difficult to measure. To date, these parameters have been used as 'fitting parameters' where the model works back from measured thermal data to obtain a reasonable simulated thermal field. While this approach is useful for creating process models to predict, for example, residual stresses it is less useful for providing insights into the process itself. Mathematical approximations for the total heat generated by the tool shoulder may be used to compensate for deformation heat generation; this could be done by an adjusting coefficient of friction. Friction is a complex physical phenomenon that depends on parameters like material, surface roughness, lubrication, temperature and pressure. The effects of friction in metal forming simulations are commonly accounted for by Coulomb friction models [26]. Assuming slipping conditions, the friction coefficient is adjusted in order to calibrate the model. A wide range of published values for friction coefficient is within 0.3-0.85 [26], which reflect the experimental conditions.

Total frictional heat of shoulder at rubbing angular speed of$(1-\delta)\omega$, will be:

$$Q_s = \frac{2}{3}\pi(1-\delta)\omega\mu P R_s \quad (10)$$

where δ is the slip factor that compensate for tool/material relative velocity. Typical values for slip factor found in literature ranges between 0.6, 0.85 [26].

In similar concept, heat generated by lateral surface of the pin is:

$$Q_p = 2\pi(1-\delta)\ \omega\ \mu\ P L_p\ R_p^2 \quad (11)$$

Total frictional heat generated by the tool is the summation of equations (4) and (5) which is:

$$Q_T = 2\pi(1-\delta)\omega\mu P\left(\frac{R_s^3}{3}+L_p\ R_p^2\right) \quad (12)$$

2.7 Thermo-mechanical model

The second step in the thermomechanical analysis is development of the mechanical model. The temperature distributions obtained from the thermal analysis are used as input to the mechanical model. This model is used to estimate the weld induced residual stresses. The mechanical model developed for the analysis is described in this section.

2.8 Assumptions

The following assumptions have been made in developing the structural model:

a) Deformation occurs symmetrically along the weld line, so only half of the workpiece is modeled.
b) The plate material is homogeneous.
c) The effect of creep is neglected because there is no cyclic thermal load involved.

In the present thermomechanical analysis, the incremental theory of plasticity is employed. The plastic deformation of the material is assumed to obey Von-Mises yield criterion, the associated flow rule and the work hardening rule. This assumption is made based on the assumption made by Zhu and Chao [28] in their study. Accordingly, a bilinear isotropic hardening model (BISO), provided by ANSYS® software is used. A BISO model incorporates Von-Mises yield criteria, and associated flow rules coupled with isotropic work hardening rule. In the model, the stress-strain behavior is described by bilinear stress-strain curves. Figure (7) presents the yield stress, Young's modulus and thermal expansion coefficient and ultimate stress of Al 7020-T53 at various temperatures are used in all calculations to consider the effect of strain hardening on the residual stresses.

The element "SOLID45" is used for the 3-D modeling of the solid structures. The element is defined by eight nodes having three degrees of freedom at each node: translations in the nodal x, y, and z directions. Geometry of "SOLID45" is the same of element "SOLID70" [23].

In order to define the temperature dependent properties, combination of MPTEMP and MPDATA commands was used. MPTEMP was used to define a series of temperatures, and later MPDATA was used to define corresponding material property values.

2.9 Boundary conditions

In the present analysis, sequentially coupled finite element analysis is carried out. The temperature histories obtained from thermal analysis are applied as body loads in the mechanical analysis. The forces from the thermal expansion of the workpiece material are the only forces considered in this analysis.

The following boundary conditions are utilized for the mechanical analysis:

a) The workpiece is constrained of vertical motion at the bottom surface.
b) The workpiece is fixed through clamping by carbon steel strip (250mm, 40mm and 30mm) totally rigid boundary conditions are applied at these clamping locations. The clamping constraints are released after the weld cools down to room temperature.
c) There are no displacements along the symmetric surface.

2.10 Simulation

The thermomechanical modeling was carried out in two stages. Transient thermal analysis is the first stage followed by nonlinear transient structural analysis in the second stage. Figure-8 illustrates the flow diagram of the method used for the finite element analysis. Since the problem involves nonlinear analysis, full Newton-Raphson option was used to solve the nonlinear equations.

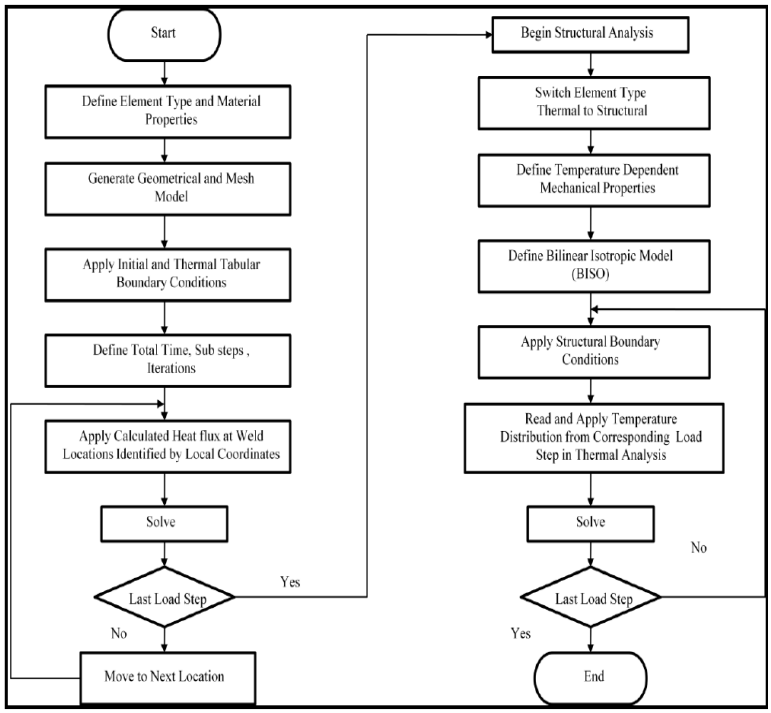

Figure-8. Flowchart of sequentially coupled thermomechanical analysis.

3. RESULTS AND DISCUSSIONS

3.1 Axial force measuring

Experiments are conduct under different welding rotational speed in order to use the measured vertical loads for verification of the accuracy of the modeled ones.

Four cases are considered with differing tool rotational speeds (710rpm, 900rpm, 1120rpm and 1400rpm) it used for measuring the vertical force during the FSW process for penetration time 60sec after that tool is moving with constant travel speed. Figure-9; shows the vertical force measured from FSW process for different tool rotational speed. Increasing of rotational speed decrease in axial force because decreasing in strength of material under the tool due to friction heat generation between tool and workpiece.

In Figure there are two stage represented first stage when tool pin penetrate in the workpiece 20sec the load comes to maximum value, temperature increase but few friction area around the pin surface therefore workpiece material strengthen the tool axially movement after that time tool was penetrated at 30sec the load decrease because the temperature increase so that the strength (mechanical properties) is function of temperature at time 40sec the shoulder surface contacted with workpiece the temperature increased comes to maximum value because the heat generated by the friction of shoulder surface and the material stirring around the pin, this behavior of axial load agreement with Soundararajan, V *et al* [24] and Muhammed A.M. *et al* [31] force measuring results.

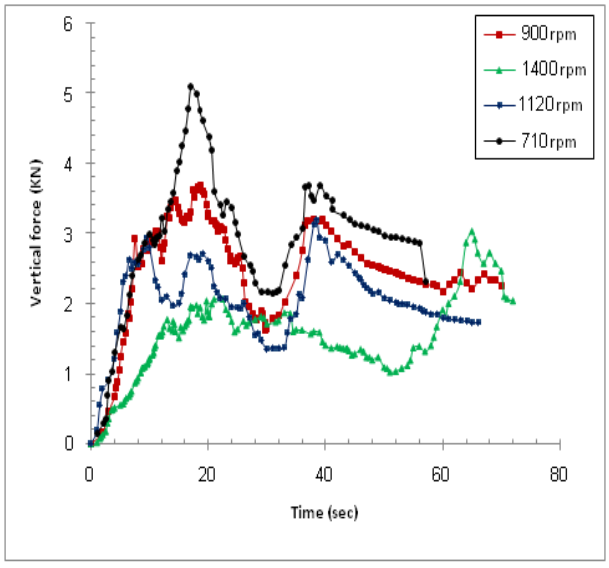

Figure-9. Vertical force penetration of tool on the workpiece during the FSW process.

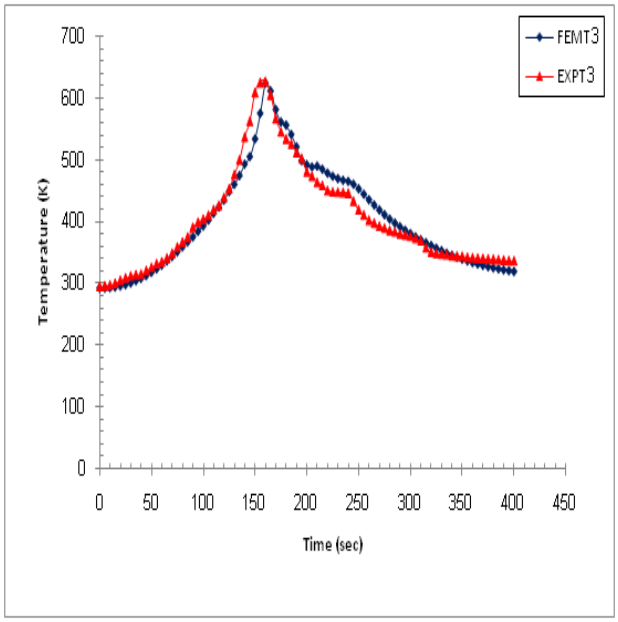

Figure-10. Comparison of the modeled and measured temperature history for thermocouple T3 location 7mm from joint line on advance side in section B-B.

3.2 Temperature curve of FSW process:

During the penetration phase, the rotating tool pin penetrates into the workpiece until the tool shoulder comes contact with the workpiece. The penetration speed is chosen to be (0.0783mm/sec) in the model, and the corresponding penetration time is approximately (80sec). convection heat transfer coefficient with backing plate ($300W/m^2k$), convection heat transfer coefficient($30W/m^2k$), ambient and initial temperature (T_o=293K), slip factor (δ=0.6), friction coefficient (μ=0.41), (axial load=2kN) , Heat generation (Q=331watt) used as input welding parameters in the finite element calculation with their corresponding vertical force in the workpiece predicted in Figure-9 the plasticization of material under the tool increase with increase rotational speed and with decrease in tool traverse speed resulting the reduction of vertical force [31].

The finite element simulation couples the moving tool with the workpiece and also considers the thermal effect of the initial tool pin penetration before start of the weld

Figure-10 shows comparison of experimental value and F.E modeled value for thermocouple T3 in section B-B while the tool traveled at mid position along tool movement in welding line at time 160sec.

Figure-11 shows that peak temperature resulting from transient thermal modeling analysis is more than experimental results because of the lake of accuracy in modeling of heat transfer. In actual case heat transfer through the fixture will increase the cooling process of the workpiece. The results obtained from transient thermal modeling were more accurate for workpiece of small dimensions relative to the heat source. Section B-B located at middle position at y=76.5mm, four thermocouples two (T3 &T4) in advance side and two (T9&T10) in retreate

side, T3 and T9 located in 7mm in transverse of welding line (under shoulder surface when tool pass over this area).

Experimentally result shows the temperature in advance side is higher than retreate side because material flow and plastic deformation around tool moving from advance side to retreate side additional to friction heat under the shoulder that gives higher temperature the computational results show that the material flows on the retreating and the front sides are higher. So, the slipping rates on the retreating and the front sides are lower than the ones on the trailing and advancing sides. This is the reason that the heat fluxes on the trailing and the advancing sides are higher, which leads to the fact that the temperatures are higher in this region for both thin and thick plates. Also the peak temperature on the advancing side is slightly higher by 10–15 ^{o}K compared to that of the retreating side, it is caused by the tangential velocity vector whose direction is the same as the forward velocity vector on the advance side, but the corresponding direction is contrary to the forward velocity vector on the retreate side.

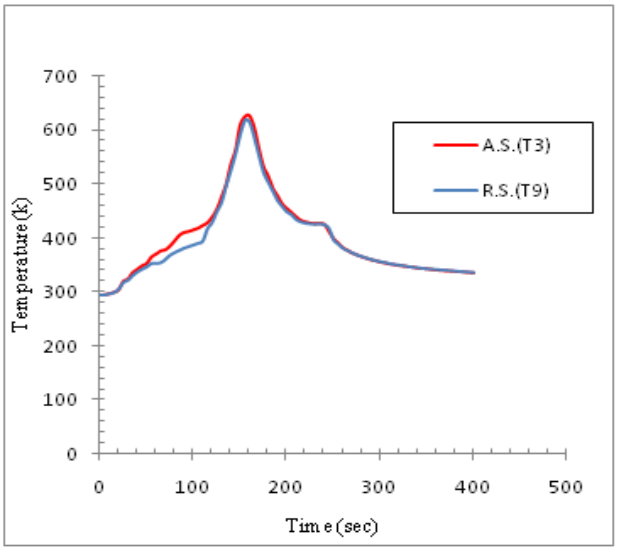

Figure-11. Comparison thermocouples measured value in advance T3 and retreate side T9 at section B-B (ω=1400rpm and V_t=40 mm/min).

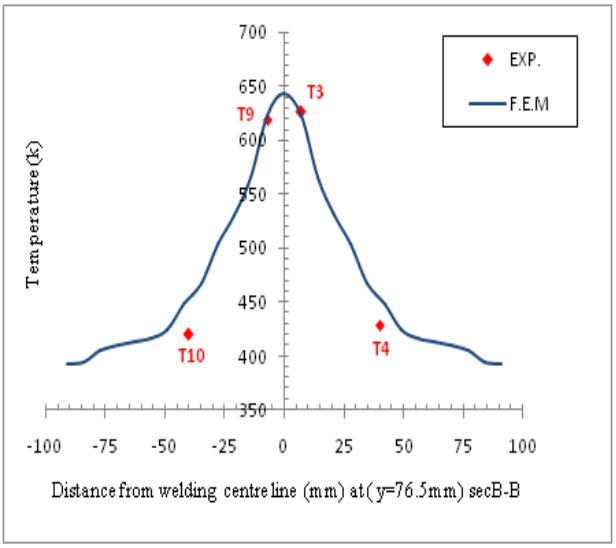

Figure-12. Comparison of F.E.M value and measured temperature distribution of along transverse direction welding line at sec.B-B (ω=1400rpm and V_t=40 mm/min).

Figures-13 shows finite element modeling of the distribution of temperature in the transverse direction of welding line in the section B-B when welding tool at mid position of workpiece and according to assumption symmetric value in advance and retreate side T_{max}=642K for (1400rpm-40mm/min).Figures shows temperature modeled and measured at section B-B when tool position at mid welding line with time 160sec, thermocouples T3, T4 in advance side and T9, T10 in retreate side (the letter T refer to thermocouple number and position), the thermocouples placed at depths 0.5mm below the top surface thermocouple reading shows temperature in advance (T3=626.6K) is larger than retreate side (T9=609.1K).

Figure-14 shows modeling thermal distribution when the tool moving along welding line at mid position of the workpiece at time 160sec, the temperature distribution effected by heat conduction between the work piece with fixture and by convection, radiation ambient travel speed also has influence on temperature distributions travel speed and rotating speed on transient temperature distribution.

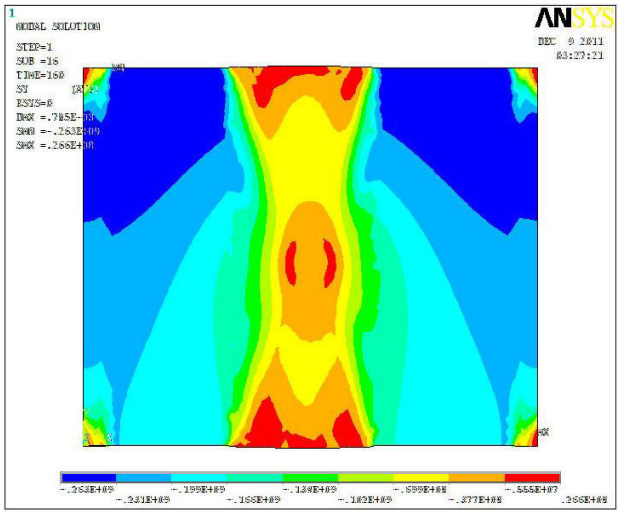

Figure-13. Stresses Distribution contour in Y direction on the top surface of the workpiece at the movement the tool moves to the middle point of the plate (ω=1400rpm and V_t=40 mm/min) at time (160 sec).

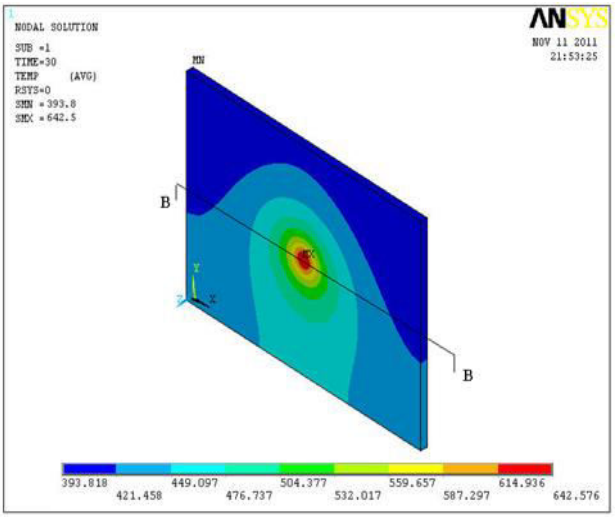

Figure-14. Temperature gradient contour in the top surface of the workpiece at the movement the tool moves to the middle point of the plate (ω=1400rpm and V_t=40 mm/min) at time (160sec) [31].

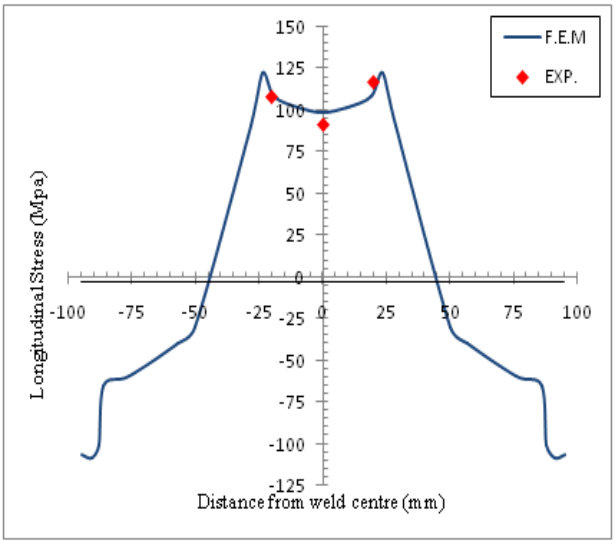

Figure-15. Experimental vs. finite element model longitudinal residual stress distribution in a transverse section at 1400 rpm and 40 mm/min.

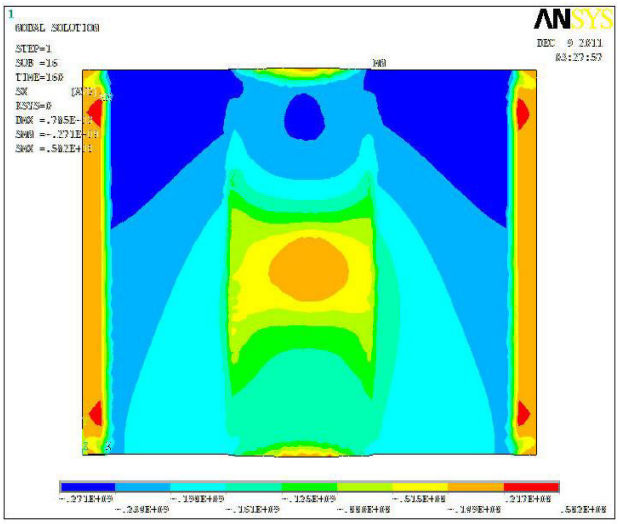

Figure-16. Stresses Distribution contour in X direction on the top surface of the workpiece at the movement the tool moves to the middle point of the plate (ω=1400rpm and V_t=40 mm/min) at time (160 sec).

Figure-15 shows the stress profile of the welded plate in the longitudinal direction (Y direction), When the tool reaches the middle of the workpiece .It can be seen that the stress distribution in front of the plate is very high as it has been affected by thermal stress and by structural loading. In the area near front and behind tool, it is observed that the tensile stress starts to increase due to the mechanical force in the horizontal direction and reaches maximum at the tool especially at sides' tool. The region side the tool under clamp has a compressive stress with the maximum value just front the clamps. The thermal expansion and constraint on the sides by the fixture results in compressive stress in this area. This stress extends to the region near the edge behind the tool. In the region marked behind the tool, the compressive stress changes

into tensile stress due to the contraction of the workpiece as it cools, which is restricted by the fixture clamps to either side of the weld.

In Figure-16, the active stress in the transverse direction is shown (X direction). There is very little tensile stress as compared with longitudinal stress, the area front and behind the tool has a high compressive stress because of the thermal stress leading to expansion of workpiece which is constrained by the fixture on both sides. The area near to the tool in the transverse direction as the stress development is due to tool movement along the Y axis, which mainly affects stress creation in the longitudinal direction has a tensile stress as the shrinkage of the workpiece has started to take place with constraints at the ends.

Figure-17 shows that the experimental stresses longitudinal and transverse at section B-B, the measured residual stress values present longitudinal stress higher than transverse stress three positions of strain gauges, also it observed that the stresses in advance side is higher that retreate side according to temperature gradient difference along welding sides with thermocouples T3, T4, T9 and T10 reading as shown in Figure-13.

The tensile residual stress presents in the weld zone, i.e. weld nugget zone, mechanical-thermal zone and heat-affected zone. In agreement with stress balance, Overall, the residual stresses have the conventional ‘‘M’’ profile with tensile stress peaks in the heat-affected zone outside the weld, which is in agreement with [30]. This is due to the tool action which strains and heats the material. As the cooling starts, the surrounding material without softening does not allow the plastic material to recover the strains, the tensile residual stress and compressive residual stress presents in the weld zone and base material, respectively. Compared to the other weld zone, the plastic extent of material mixing in the stir zone improves and the resistance of dislocation motion reduces, resulting in residual stress relaxation. So the longitudinal residual stress presents an ‘‘M’’ profile. Meanwhile, the profiles are slightly asymmetric in the advancing side and retreating side, which reflects the somewhat asymmetric nature of the friction stir welding process. The advancing and retreating sides of the weld correspond to where the maximum and minimum relative velocities between the tool and work-piece are observed. The material experiences the role of longitudinal tensile on the advancing side which is moving in the same direction as the tool translation, and then produces the longitudinal mechanical tensile stress. This is in contrast to the material on the retreating side. The largest value of tensile longitudinal residual stress experimentally (up to 116 MPa) are obtained at the highest rotary speed of 1400 rpm, occurring at the edge of the shoulder on the advancing side, with a value (32%) of the yield strength of the base material (365 MPa) Figure-17 and Figure-18 shows good agreement F.E.M values with measured value for longitudinal stress and transverse stress.

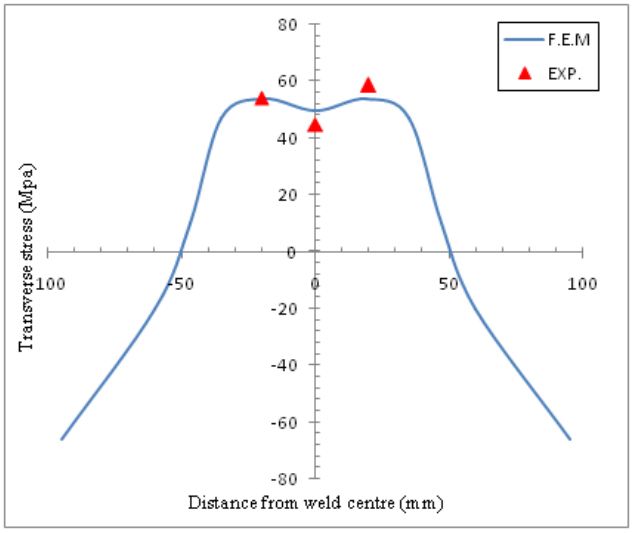

Figure-17. Experimental vs. finite element model traverse residual stress distribution in a transverse section at 1400 rpm and 40 mm/min.

4. CONCLUSIONS

In this paper, a systematic numerical analysis using ANSYS-software and experimental analysis transient thermal distribution using thermocouples and residual stresses by the hole-drilling strain-gauge method in friction stir welded 5 mm plates of 7020-T53 allow several conclusions to be drawn.

- Axial load that measured from experimental work decrease with increase rotational speed because that decrease in strength due to temperature increases in penetration position.
- The experimental data show the maximum temperature measured during FSW at mid position 629k and numerically value from the simulation is 642k^{o}, which is significantly less than the melting temperature of 7020-T53 aluminum alloy at 916K^{o}.
- The temperature measured at advance side (629k) is higher than retreate side (605k).
- Numerical results (Tmax =642K) agreement with measured data (Tmax=629k) (error 2%).
- Numerical results of residual stresses on the top surface has the conventional ‘‘M’’ profile with tensile stress peaks in the heat-affected zone outside the weld and the longitudinal residual stress measured is asymmetric with respect to the weld centerline and shows good agreement F.E.M values with measured value for longitudinal stress and transverse stress.
- Experimental results shows the largest value of tensile longitudinal residual stress experimentally (up to 116 MPa) are obtained at the highest rotary speed of 1400 rpm, occurring at the edge of the shoulder on the advancing side, with a value (32%) of the yield strength of the base material (365 MPa).

REFERENCES

[1] Zhang Z, Zhang HW. 2008. A fully coupled thermo-mechanical model of friction stir welding. Int J Adv Manuf Technol. 37: 279-293.

[2] Cho JH, Boyce DE, Dawson PR. 2005. Modeling strain hardening and texture evolution in friction stir welding of stainless steel. Mater Sci Eng 398: 146-163.

[3] Nandan R, DebRoy T, Bhadeshia HKDH. 2008. Recent advances in friction-stir welding-process, weldment structure and properties. Prog Mater Sci. 53: 980-1023.

[4] Chao YJ, Qi X, TangW. 2003. Heat transfer in friction stir welding-experimental and numerical studies. J Manuf Sci Eng. 125: 138-145.

[5] Schmidt HB, Hattel JH. 2008. Thermal modelling of friction stir welding. Scr Mater. 58: 332-337.

[6] Mandal S, Williamson K. 2006. A thermo-mechanical hot channel approach for friction stir welding. J Mater Process Technol. 174: 190-194.

[7] Song M, Kovacevic R (2003) Thermal modeling of friction stirs welding in a moving coordinate system and its validation. Int J Mach Tools Manuf. 43: 605-615.

[8] Zhang HW, Zhang Z, Chen JT. 2005. The finite element simulations of the friction stir welding process. Mater Sci Eng. 403: 340-348.

[9] Zhang Z, Zhang HW. 2007. Material behaviors and mechanical features in friction stir welding process. Int J Adv Manuf Technol. 35: 86-100.

[10] Zhang Z, Zhang HW. 2009. Numerical studies on controlling of process parameters in friction stir welding. J Mater Process Technol. 209: 241-270.

[11] Nandan R, Roy GG, Debroy T. 2006. Numerical simulation of three-dimensional heat transfer and plastic flow during friction stir welding. Metall Mater Trans. 37A: 1247-1259.

[12] Nandan R, Roy GG, Lienert TJ, Debroy T. 2006. Numerical modelling of 3D plastic flow and heat transfer during friction stir welding of stainless steel. Sci Technol Weld Joining. 11: 526-537.

[13] John R, Jata KV, Sadananda K. 2003. Residual stress effects on near-threshold fatigue crack growth in friction stir welds in aerospace alloys. Int. J Fatigue. 25: 939-948.

[14] Bussu G, Irving PE. 2003. The role of residual stress and heat affected zone properties on fatigue crack propagation in friction stir welded 2024-T351 aluminium joints. Int J Fatigue. 25:77-88.

[15] Khandkar MZH, Khan JA, Reynolds AP, Sutton MA. 2006. Predicting residual thermal stresses in friction stir welded metals. J Mater Process Technol. 174: 195-203.

[16] Chen CM, Kovacevic R. 2003. Finite element modeling of friction stir welding-thermal and thermomechanical analysis. Int. J Mach Tools Manuf. 43: 1319-1326.

[17] Buffa G, Hua J, Shivpuri R, Fratini L. 2006. A continuum based FEM model for friction stir welding-model development. Mater Sci Eng. 419: 389-396.

[18] Rajesh SR, Bang HS, Chang WS, Kim HJ, Bang HS, Oh CI, Chu JS. 2007. Numerical determination of residual stress in friction stir weld using 3D-analytical model of stir zone. J Mater Process Technol. 187-188: 224-226.

[19] Peel M, Steuwer A, Preuss M, Withers PJ. 2003. Microstructure, mechanical properties and residual stresses as a function of welding speed in aluminium AA5083 friction stir welds. Acta Mater. 51: 4791-4801.

[20] Linton VM, Ripley MI. 2008. Influence of time on residual stresses in friction stir welds in age hardenable 7xxx aluminium alloys. Acta Mater. 56(16): 4319-4327.

[21] Peel M, Steuwer A, Preuss M, Withers PJ. 2003. Microstructure, mechanical properties and residual stresses as a function of welding speed in aluminium AA5083 friction stir welds. Acta Mater. 51(16): 4791-801.

[22] Fratini L, Pasta S, Reynolds AP. 2009. Fatigue crack growth in 2024-T351 friction stir welded joints: longitudinal residual stress and microstructural effects. Int. J Fatigue. 31(3): 495-500.

[23] ANSYS® Release 12.0 Documentation, ANSYS Inc, 2009.

[24] Soundararajan V., Zekovic, S. and Kovacevic R. 2005. Thermo-mechanical model with adaptive boundary conditions for friction stir welding of Al 6061. International Journal of Machine Tools and Manufacture. 45(14): 1577-1587.

[25] 2005. Standard Test Method for Determining Residual Stresses by the Hole-Drilling Strain-Gage Method. ASTM standard, Volume 03.01, Section 03.

[26] Sarmad Dhia Ridha. 2010. An investigation of friction stir welding and stress relief by vibration of 6061-T6 aluminum alloy. Ph.D. Thesis, University of Baghdad.

[27] Lubarda, Vlado A. 2002. Elastoplasticity Theory. CRC Press LLC.

[28] Zhu, X.K. and Chao, Y.J. 2004. Numerical simulation of transient temperature and residual stresses in friction stir welding of 304L stainless steel. Journal of Materials Processing Technology. 146(2): 263-272.

[29] 1992. Properties and Selection: Non-Ferrous Alloys and Special Purposes Materials. ASM Handbook, American Society for Metals. Vol. 2.

[30] Prime Michael B, Gnaupel-Herold Thomas, Baumann John A, Lederich Richard J, Bowden David M, Sebring Robert J. 2006. Residual stress measurements in a thick, dissimilar aluminum alloy friction stir well. Acta Mater. 54(15): 4013-4021.

[31] Muhsin J. J., Moneer H. Tolephih and Muhammed A. M. 2012. Effect Of Friction Stir Welding Parameters (Rotation And Transverse) Speed On The Transient Temperature Distribution In Friction Stir Welding Of AA 7020-T53. ARPN Journal of Engineering and Applied Sciences. 7(4).